THE JOURNAL OF PHYSICAL CHEMISTRY A

Article

pubs.acs.org/JPCA

Optimization of the Double Pump–Probe Technique: Decoupling the Triplet Yield and Cross Section

Davorin Peceli,[†] Scott Webster,[†] Dmitry A. Fishman,[†] Claudiu M. Cirloganu,[†] Honghua Hu,[†] Olga V. Przhonska,[†,§] Vladimir V. Kurdyukov,[∥] Yurii L. Slominsky,[∥] Alexey I. Tolmachev,[∥] Alexey D. Kachkovski,[∥] Raghunath R. Dasari,[⊥] Stephen Barlow,[⊥] Seth R. Marder,[⊥] David J. Hagan,[†,‡] and Eric W. Van Stryland*[,†,‡]

[†]CREOL: College of Optics and Photonics, and [‡]Department of Physics, University of Central Florida, Orlando, Florida 32816, United States

[§]Institute of Physics, National Academy of Sciences, Kiev 03028, Ukraine

[∥]Institute of Organic Chemistry, National Academy of Sciences, Kiev 03094, Ukraine

[⊥]School of Chemistry and Biochemistry, Georgia Institute of Technology, Atlanta, Georgia 30332, United States

Supporting Information

ABSTRACT: The double pump–probe technique (DPP), first introduced by Swatton et al. [*Appl. Phys. Lett.* **1997**, *71*, 10], is a variant of the standard pump–probe method but uses two pumps instead of one to create two sets of initial conditions for solving the rate equations, allowing a unique determination of singlet- and triplet-state absorption parameters and transition rates. We investigate the advantages and limitations of the DPP theoretically and experimentally and determine the influence of several experimental parameters on its accuracy. The accuracy with which the DPP determines the triplet-state parameters improves when the fraction of the population in the triplet state relative to the ground state is increased. To simplify the analysis of the DPP, an analytical model is presented, which is applicable to both the reverse saturable and the saturable absorption regimes. We show that the DPP is optimized by working in the saturable absorption regime. Although increased accuracy is in principle achievable by increasing the pump fluence in the reverse saturable absorption range, this can cause photoinduced decomposition in photochemically unstable molecules. Alternatively, we can tune the excitation wavelength to the spectral region of larger ground-state absorption, to achieve similar accuracy. This results in an accurate separation of triplet yield and excited-state absorption cross section. If the cross section at another wavelength is then desired, a second pump–probe experiment at that wavelength can be utilized given the previously measured triplet yield under the usually valid assumption that the triplet yield is independent of excitation wavelength.

1. INTRODUCTION

Organic and metal–organic materials with singlet ground states and fast intersystem crossing (ISC) rates to form triplet excited states are of interest for many applications including optical limiting of long optical pulses,[1−3] phosphorescent organic light-emitting diodes (P-OLEDs),[4,5] phosphorescent materials for investigating biological systems,[6] phosphorescence resonance energy transfer,[7] and photodynamic therapy.[8−11] The accurate determination of the triplet quantum-yield, ϕ_T, which gives the fraction of excited molecules decaying to the triplet state as compared to those remaining in the lowest singlet excited state and subsequently decaying to the singlet ground state, is important in characterizing the photophysics of such materials. Some of the most frequently used experimental techniques for ϕ_T determination are: (1) photoacoustic calorimetry;[12] (2) generation of singlet oxygen ($^1O_2$);[13] and (3) singlet-state depletion.[14,15] Photoacoustic calorimetry[16] is based on a measurement of the heat that is released from a sample after nonradiative relaxation and requires accurate knowledge of the energy of the triplet state and fluorescence quantum yield. $^1O_2$ generation[13] relies on quenching of sufficiently energetic (>0.978 eV) molecular triplet states by ground-state $^3O_2$ to form $^1O_2$. The quantum yield of $^1O_2$ generation, Φ_Δ, is typically determined through comparison of $^1O_2$ luminescence of the sample with that of a known reference material (usually acridine in acetronitrile with a generally accepted Φ_Δ of ∼0.82); from the concentration of molecular oxygen in solution and Φ_Δ, it is possible to determine ϕ_T. Singlet-state depletion, also referred to as ground-state recovery,[14,15] is a transient absorption technique using a single pump pulse and a weak probe at the same wavelength, in a spectral region where there is strong saturable absorption (SA). If the triplet–triplet (TT) absorption at that particular wavelength can be ignored, this method can yield accurate results for ϕ_T. However, for many molecules, TT absorption in the SA regime is significant[17] and without a priori knowledge of the triplet absorption cross

Received: February 1, 2012
Revised: April 24, 2012
Published: April 26, 2012

   dx.doi.org/10.1021/jp301051u | *J. Phys. Chem. A* 2012, 116, 4833–4841

section, σ_T, in this region, large errors in determining ϕ_T are often encountered, as demonstrated in the Experimental Section.

The double pump−probe technique (DPP) introduced by Swatton et al.[18] has the advantage of allowing for the determination of the triplet quantum yield, ϕ_T, while not requiring the use of a reference sample, and also allows for the determination of σ_T, in the same experiment. The fundamental concept of the DPP is to pump the sample under investigation with two strong pump pulses (usually, but not necessarily, having the same pulse energies, E_i) separated by a time delay chosen to allow for significant depopulation of the singlet excited states via decay to the singlet ground state or via ISC to the triplet state. The experimental setup is shown in detail in section 3. Typically, although not necessarily, equal wavelengths are used for both pumps and probe to reduce the number of unknown variables in the analysis. Because of spin-selection rules, the triplet lifetimes are always significantly longer than singlet lifetimes; thus, the second pump encounters a different population distribution than that encountered by the first pump. Specifically, the second pump sees a larger population in the lowest-lying triplet state and a smaller population in the ground state.

There have been several reports of measurements on organic compounds using DPP;[19−21] however, there are limitations to its accuracy, which we identify and resolve in this work. For some applications, such as optical limiting, there is a need to perform measurements in the reverse saturable absorption (RSA) regime, a region where the excited-state absorption (ESA) cross section is larger than the ground-state absorption cross section. The creation of a significant molecular triplet-state population in the RSA region requires large pump fluence, which can lead to dye photodecomposition. Although lowering the pump fluence and increasing the dye concentration may lead to the same signal-to-noise ratio, we show that the sensitivity of the DPP for separately determining ϕ_T, and σ_T, is greatly reduced. We also show that working in the saturable regime can greatly increase this sensitivity, although it requires a second experiment if the cross section is needed at a wavelength in the RSA regime.

In this work, we systematically study the influence of different experimental parameters, such as pump fluence (F), dye concentration, and pump wavelengths (relative to the linear absorption peak within the SA and RSA regimes), on the accuracy and optimization of DPP. Our theoretical and experimental studies show that for photochemically unstable materials, which do not allow for the use of high pump fluences, accuracy is significantly increased by utilizing small dye concentrations (1−10 μM, for molecules with peak molar absorptivities of $\varepsilon_{max} \sim 10^5$ M^{-1} cm^{-1}) and by shifting the pump wavelength to the SA region to significantly deplete the ground-state population. Our optimized DPP effectively utilizes the most desirable attributes of the DPP and singlet-state depletion techniques.

2. THEORETICAL BACKGROUND

The standard five-level energy diagram describing light absorption and emission of organic molecules with singlet−singlet (SS) and TT transitions and their relaxation processes is presented in Figure 1. It is well-known that there are several competing processes to depopulate the S_1 state, which include: (1) radiative (fluorescence) and nonradiative decay (internal conversion) into the singlet ground state (S_0) with lifetime τ_{S10};

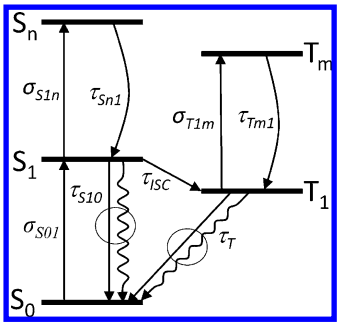

Figure 1. Energy level diagram of a five-level system of singlet and triplet transitions. S_0, S_1, and S_n are singlet, while T_1 and T_m are triplet electronic energy levels. σ_{ij} and τ_{ij} are cross sections and lifetimes pertaining to the particular singlet and triplet transitions, respectively. As indicated by the circles, τ_{S10} and τ_T include both radiative and nonradiative decays.

(2) excitation to the higher-lying singlet states (S_n) by sequential absorption of another photon; and (3) ISC leading to population of a triplet state (usually the lowest triplet manifold, T_1, although exceptions exist[22−24]) with lifetime τ_{ISC}. The singlet lifetime, τ_S, can be written as: $1/\tau_S = 1/\tau_{S10} + 1/\tau_{ISC}$. The decay from T_1 to S_0 can also follow a nonradiative or radiative (phosphorescent) pathway; however, the lifetime of the T_1 state is long (usually 10^{-8} to 10^2 s) due to the spin-forbidden nature of a triplet−singlet transition.

The propagation and rate equations for the full five-level system are described in eqs 1 and 2:

$$\frac{dI}{dz} = -\sigma_{S01}N_{S0}I - \sigma_{S1n}N_{S1}I - \sigma_{T1m}N_{T1}I \quad (1)$$

$$\frac{dN_{S0}}{dt} = -\frac{\sigma_{01}N_{S0}I}{\hbar\omega} + \frac{N_{S1}}{\tau_{S10}} + \frac{N_{T1}}{\tau_T}$$

$$\frac{dN_{S1}}{dt} = \frac{\sigma_{01}N_{S0}I}{\hbar\omega} - \frac{N_{S1}}{\tau_{S10}} - \frac{\sigma_{S1n}N_{S1}I}{\hbar\omega} + \frac{N_{Sn}}{\tau_{Sn1}} - \frac{N_{S1}}{\tau_{ISC}}$$

$$\frac{dN_{Sn}}{dt} = \frac{\sigma_{S1n}N_{S1}I}{\hbar\omega} - \frac{N_{Sn}}{\tau_{Sn1}}$$

$$\frac{dN_{T1}}{dt} = -\frac{\sigma_{T1m}N_{T1}I}{\hbar\omega} + \frac{N_{Tm}}{\tau_{Tm1}} + \frac{N_{S1}}{\tau_{ISC}} - \frac{N_{T1}}{\tau_T}$$

$$\frac{dN_{Tm}}{dt} = \frac{\sigma_{T1m}N_{T1}I}{\hbar\omega} - \frac{N_{Tm}}{\tau_{Tm1}} \quad (2)$$

where I is the irradiance, z is the depth in the sample, and N_{S0}, N_{S1}, N_{Sn}, N_{T1}, and N_{Tm} are populations in the singlet S_0, S_1, and S_n and triplet T_1 and T_m states, respectively. τ_S and τ_T are the fluorescence and phosphorescence lifetimes (both including radiative and nonradiative decays). The total population, $N_{TOT} = N_{S0} + N_{S1} + N_{Sn} + N_{T1} + N_{Tm}$, $N_{TOT} = N_{S0} + N_{S1} + N_{Sn} + N_{T1} + N_{Tm}$, is conserved at all times.

To mathematically describe the physical processes presented in Figure 1, the propagation and rate equations (eqs 1 and 2)[25] are utilized. The triplet quantum yield is defined as:

$$\phi_T = \frac{\tau_S}{\tau_{ISC}} = \frac{\tau_{S10}}{\tau_{S10} + \tau_{ISC}} \quad (3)$$

Because the lifetimes τ_{Sn1} and τ_{Tm1} are usually short (subpicosecond), the modeling of ESA dynamics can be simplified by disregarding the populations of the higher-lying

dx.doi.org/10.1021/jp301051u | J. Phys. Chem. A 2012, 116, 4833−4841

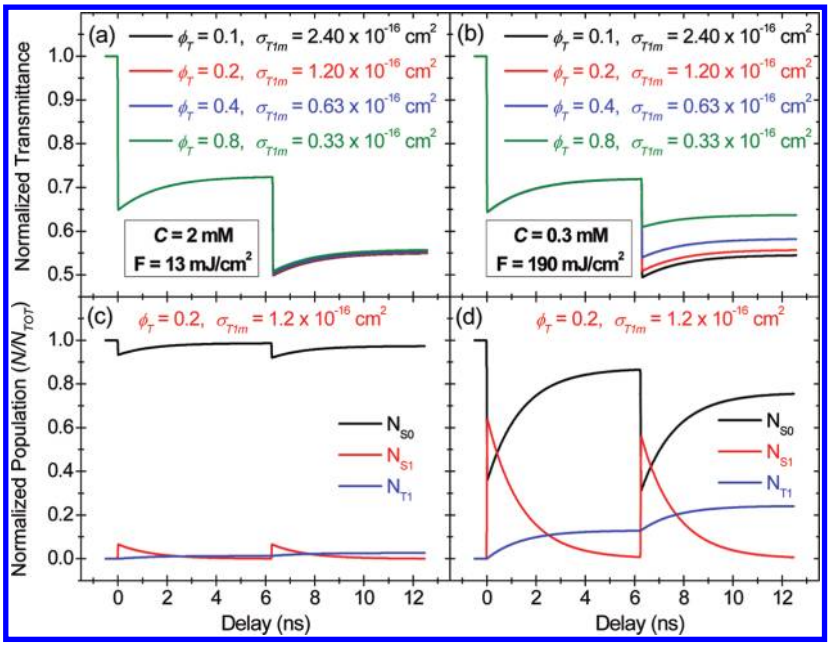

Figure 2. (a,b) Numerical simulation of DPP dynamics shown as normalized transmittance versus time delay between pump and probe pulses for SiNc at 532 nm with parameters for different ϕ_T and σ_{T1m}. Using $\kappa = +22 \times 10^{-18}$ cm^2, $\sigma_{S01} = 2.8 \times 10^{-18}$ cm^2, and $\sigma_{S1n} = 32 \times 10^{-18}$ cm^2, (a) $T_L = 0.6$ ($C = 2$ mM) with an input fluence of $F = 13$ mJ/cm^2 in each pump and (b) $T_L = 0.95$ ($C = 0.3$ mM) with an input fluence of $F = 190$ mJ/cm^2 in each pump. (c,d) Population dynamics for the ground (N_0), first excited singlet (N_{S1}), and triplet (N_{T1}) states using $\phi_T = 0.2$ and $\sigma_{T1m} = 1.2 \times 10^{-16}$ cm^{-2} for the two cases of DPP simulation in (a) and (b), respectively.

singlet (S_n) and triplet (T_m) states. Note that, in most cases, with excitation pulses shorter than ~10 ns and pulse repetition rates less than tens of kilohertz, the rate of the triplet-state depopulation, $1/\tau_T$, is also neglected in modeling. The set of eqs 1 and 2 can be solved for the first pump pulse yielding a unique solution for the constant κ connecting ϕ_T and σ_{T1m} (derivation provided in the Supporting Information) in the form:

$$\kappa = \phi_T \cdot (\sigma_{T1m} - \sigma_{S01}) \tag{4}$$

Note that in the SA and RSA regimes κ is negative and positive, respectively. To decouple the two molecular parameters ϕ_T and σ_{T1m}, numerical fitting of the rate equations must be repeated for the second pump pulse.[18] Usually, delay between the two pumps is chosen to allow for nearly complete depopulation of the first singlet state. However, this is not a requirement, and the lifetime of S_1 can still be determined by solving the rate equations for shorter delays between the two pumps. Because the lifetime of T_1, τ_T, is typically much longer than the temporal separation between the two pump pulses, the triplet-state population produced by the first pump can be considered constant. The second pump interacts with the modified molecular system, and the initial conditions for solving the rate equations are different. Numerical solution of the rate equations in Figure 2b for the transmittance change due to the second pump together with the solution of eq 4 obtained from the first pump allows for a unique determination of ϕ_T and σ_{T1m}. For most molecules, we may use pulses of a few picoseconds in duration, but for molecular systems with ultrafast ISC rates,[26−28] femtosecond pulses may be required to determine ϕ_T and σ_{T1m} separately.[29]

Examples of the numerical simulations of DPP dynamics, allowing the decoupling of the two molecular parameters ϕ_T and σ_{T1m}, are shown in Figure 2 for two concentrations and corresponding fluences that yield the same transmittance change. The corresponding population dynamics are below each case shown in Figure 2a and b. We use the singlet-state parameters of a silicon naphthalocyanine derivative (SiNc) (detailed description given in section 3) at 532 nm: $\sigma_{S01} = 2.8 \times 10^{-18}$ cm^2 and $\sigma_{S1n} = 32 \times 10^{-18}$ cm^2.[18,30,31] At this wavelength, the linear absorption is small so that $\sigma_{S1n} > \sigma_{S01}$, corresponding to RSA. Additionally, on the basis of previous single pump−probe measurements of SiNc, it is known that $\kappa = 22 \times 10^{-18}$ cm^2. In all of the curves shown in Figure 2, we use this same value of κ, but different combinations of ϕ_T and σ_{T1m} that give this value of κ. Note that the probe transmittance prior to the second pump is independent of the variations in these combinations, thus indicating that in experiments, the transmittance changes induced by the first pump unambiguously give κ, but do not uniquely specify ϕ_T or σ_{T1m}. However, after the second pump, the probe transmittance from eqs 1and 2 depends on ϕ_T and σ_{T1m} individually.

From the results shown in Figure 2, an increase of ϕ_T for the second decrease in transmittance corresponds to a smaller value of σ_{T1m} to keep κ constant. In Figure 2a, where the concentration is large and the pump fluence is small, it is seen that the probe transmittance after the second pump pulse is relatively insensitive to changes of ϕ_T, and thus a unique determination of ϕ_T and σ_{T1n} without large errors becomes impossible. This can be understood by observing the population dynamics. In Figure 2c, we see that for the conditions of Figure 2a only a small fraction of population is transferred to T_1; therefore, ϕ_T cannot be determined with significant accuracy. Altering the measurement conditions by decreasing the concentration and pumping with larger fluences results in a significant population of the triplet states, allowing ϕ_T and σ_{T1m} to be uniquely determined, as can be seen in Figure 2b and d. Hence, an experiment conducted under the conditions shown in Figure 2b should allow unique determination of ϕ_T and σ_{T1n}. However, such a large fluence

dx.doi.org/10.1021/jp301051u | J. Phys. Chem. A 2012, 116, 4833−4841

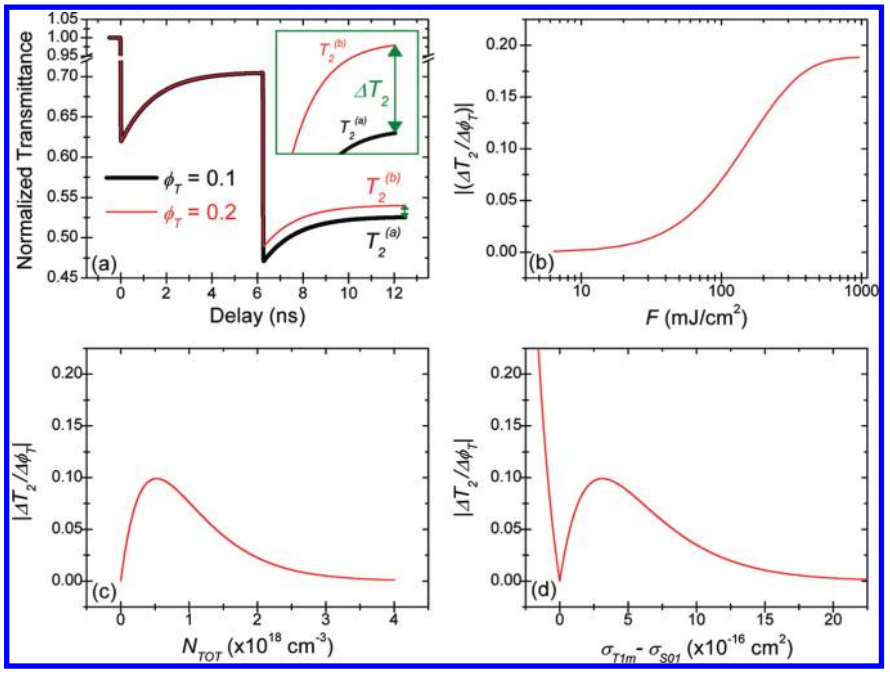

Figure 3. Solutions of rate eqs 1 and 2: (a) Plot of normalized transmittance versus delay between pump and probe pulses for the DPP in SiNc, indicating changes in transmittance $T_2^{(i)}$ with time as defined in eq 5. ΔT_2 is the difference between $T_2^{(b)}$ and $T_2^{(a)}$. The inset shows the expanded region in transmittance between $T_2^{(b)}$ and $T_2^{(a)}$. (b) $|\Delta T_2/\Delta\phi_T|$ versus input fluence at a concentration of C = 0.37 mM, (c) $\Delta T_2/\Delta\phi_T$ versus N_{TOT} with F = 190 mJ/cm^2 in each pump, and (d) $\Delta T_2/\Delta\phi_T$ versus the difference in cross sections $\sigma_{T1m} - \sigma_{S01}$ at C = 0.37 mM and F = 190 mJ/cm^2 in each pump.

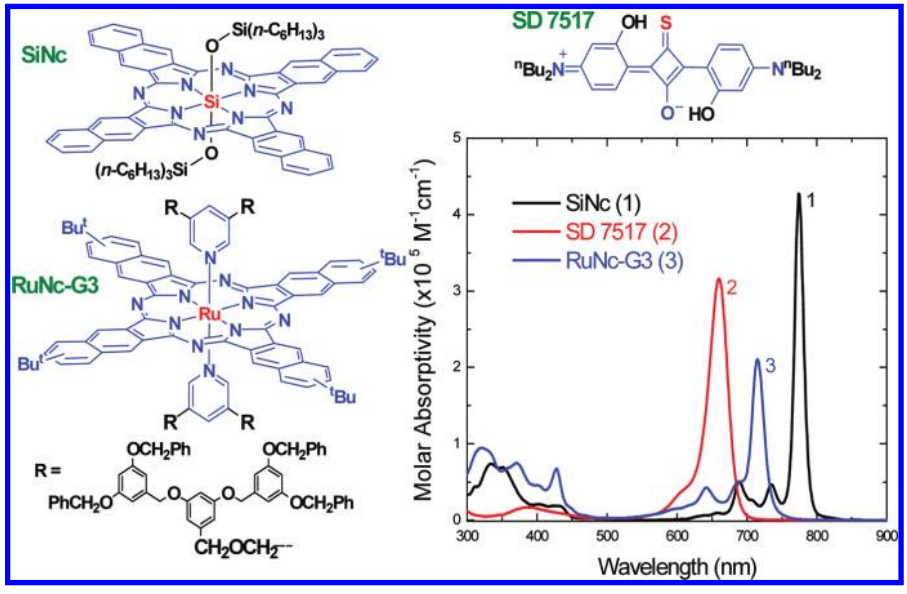

Figure 4. Molecular structures and molar absorptivity spectra of SiNc in toluene (1), SD 7517 in acetonitrile (2), and RuNc-G3 in toluene (3).

is not always practical due to photoinduced decomposition of some dyes, and may not be available (especially when using an Optical Parametric Generator/Amplifier system) due to insufficient laser output energy, E.

The sensitivity of the DPP can be quantified as the change in transmittance after the second pump (ΔT_2) with respect to a change of ϕ_T, that is, $\Delta T_2/\Delta\phi_T$ as shown schematically in Figure 3a, where we use the parameters for SiNc at 532 nm, keeping κ constant while varying ϕ_T. Insight into the influence of the experimental parameters, such as dye concentration, pump fluences, and excitation spectral region, on the accuracy of the DPP is gained. By using a simplified analytical approach with the assumption that $\sigma_{S1n} \ll \sigma_{S01}$ (otherwise the rate equations have to be solved numerically), only two competing processes are considered, ground-state absorption and TT reabsorption. We can also ignore the population of S1 for small dye concentrations where the ESA does not deplete the pump. A similar approach for an analytical solution to the rate and propagation equations was developed in previous papers[32,33] for optimizing RSA in optical-limiting studies. However, in this work, a simplified analytical solution is developed for both RSA and SA for the DPP.

dx.doi.org/10.1021/jp301051u | J. Phys. Chem. A 2012, 116, 4833−4841

Using these approximations (derivation provided in the Supporting Information), we can write an equation for $T_2^{(i)}$ corresponding to the case of complete S_1 depopulation:

$$T_2^{(i)} = \exp(-\kappa f N_{TOT}[2 - \phi_T f]L) \quad (5)$$

where $f = 1 - \exp(-\sigma_{S01}F/\hbar\omega)$ is the fraction of population that is removed from the ground state S_0 with pump excitation and L is the sample length. Differentiating T_2 with respect to ϕ_T gives the DPP accuracy:

$$\left|\frac{\Delta T_2}{\Delta \phi_T}\right| = \kappa f^2 N_{TOT} L \exp(-\kappa f N_{TOT}[2 - \phi_T f]L) \quad (6)$$

The dependence of the DPP accuracy on F and N_{TOT} is shown in Figure 3b and c, again using the parameters for SiNc (the structure of which is shown in Figure 4) at 532 nm, corresponding to the dynamics encountered under typical experimental conditions. Figure 3b illustrates increasing accuracy with larger pump fluence. However, photochemical instability of many organic molecules limits the pump fluence. Note that at $F > 400$ mJ/cm^2 this dependence tends to saturate (indicating complete depletion of the ground state); therefore, both of the above factors limit the useful pump fluence. As seen from Figure 3c, the accuracy of the DPP is low at very small concentrations, increases to a maximum, and decreases at larger concentrations, at which only a small fraction of the population moves to the triplet state. Thus, a proper choice of dye concentration is important to increase the sensitivity of the DPP.

Figure 3d shows the interesting dependence of the DPP accuracy on $\sigma_{T1m} - \sigma_{S01}$. When $\sigma_{S01} = \sigma_{T1m}$ the accuracy is zero, corresponding to the case where there is no signal because TT absorption is equal to the ground-state absorption. For small positive values of $\sigma_{T1m} - \sigma_{S01}$, corresponding to RSA, the accuracy increases to a maximum and decreases for larger values. Negative values of $\sigma_{T1m} - \sigma_{S01}$ correspond to SA. However, it is clear that if $\sigma_{S01} \gg \sigma_{T1m}$, that is, the TT reabsorption can be neglected, the second pump becomes unnecessary, and the singlet depletion technique is sufficient. Unfortunately, in general it is not known a priori if the TT can be neglected. If the excitation pump wavelength corresponds to the SA region, the singlet ground state may be considerably depleted. This will increase the triplet-state population with the use of relatively small pump fluence (~6 mJ/cm^2) and small dye concentration (~10 μM, assuming $\varepsilon_{max} \approx 10^5$ M^{-1} cm^{-1}). This leads to increased accuracy in the determination of ϕ_T and σ_{T1m} using the DPP. Note that large ϕ_T will lead to larger triplet-state population and, thus, higher accuracy of the DPP. For Figure 3b–d, ϕ_T is chosen to be 0.2.

3. EXPERIMENTAL SECTION

Materials. To demonstrate several possible situations encountered when analyzing triplet dynamics by the DPP, three different dyes were studied. We used this optimized method to characterize three organic dyes with distinct transient absorption characteristics: (1) a commercially available silicon naphthalocyanine derivative (Sigma Aldrich, CAS 92396-88-8; SiNc); (2) a new sulfur-containing squaraine (labeled as SD 7517); and (3) a recently reported dendronized ruthenium naphthalocyanine derivative (labeled as RuNc-G3).[34,35] The molecular structures and linear absorption spectra of all three dyes are shown in Figure 4.

The effect of fluence and dye concentration is shown by performing DPP measurements on the well-known triplet-forming absorber SiNc at three different concentrations in toluene. SiNc is a highly conjugated cyclic compound with a larger ϕ_T than that of metal-free naphthalocyanines due to the "heavy-atom" effect.[36] Two other samples, SD 7517 and RuNc-G3, are measured using DPP in the SA wavelength range only, as these molecules are photochemically unstable under large fluences/irradiances. In the molecular structure of the squarylium dye SD 7517, one oxygen atom in the squaraine acceptor fragment is substituted by a sulfur atom. This substitution leads to a low-lying n–π^* transition enhancing the ISC rate and ϕ_T as compared to what is seen for its all-oxygen analogue.[22] RuNc-G3 is another naphthalocyanine dye in which Ru(II) is coordinated in the center and is axially substituted with pyridine rings at the focal point of third-generation Fréchet-type dendrons. Here, a large ϕ_T is anticipated from the literature on other Ru(II) phthalocyanine and naphthalocyanine derivatives, where the ISC has been attributed to a combination of the "heavy-atom" effect and the influence of a low-lying charge-transfer state.[34−36]

Optical Setups. A detailed schematic for the DPP setup is shown in Figure 5. Picosecond measurements were performed

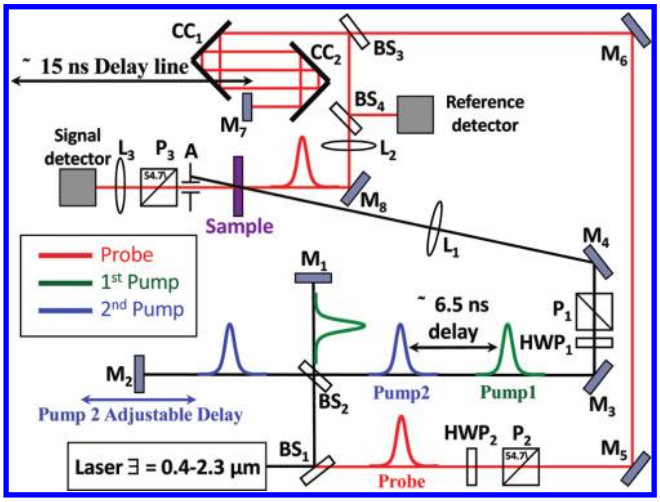

Figure 5. The DPP setup for picosecond measurements. Here, all wavelengths are the same. Line colors are used to distinguish separate pulses for clarity.

with a 10 Hz Nd:YAG laser (EKSPLA PL2143) with an optical parametric generator/amplifier (OPG/A) (PG401/DFG) tunable from 0.42 to 2.3 μm. RSA experiments used the second harmonic of the Nd:YAG laser at 532 nm with a pulse width of 22 ps (fwhm) determined by second-order autocorrelation. SA experiments were performed using the OPG/A with a pulse width of 16 ps (fwhm). Beam spot sizes (w_0) were measured with knife-edge scans at the sample position. Changes in the probe spot size with respect to delay were determined to be small due to collimation of the beam (beam diameter after spatial filter was ~2 mm HW1/e^2). The pump pulses at 532 nm had a spot size of ~75–100 μm (HW1/e^2 M), while spot sizes of the pumps coming from the OPG/A were ~220 μm (HW1/e^2 M) each. The probe spot size was less than 20 μm (HW1/e^2 M) and was contained in the central portion of the pumps' spatial profiles. The probe energy was fixed to ~200 pJ ($F \approx 0.032$ mJ/cm^2), which was small enough to prevent nonlinear effects due to the probe by

dx.doi.org/10.1021/jp301051u | J. Phys. Chem. A 2012, 116, 4833–4841

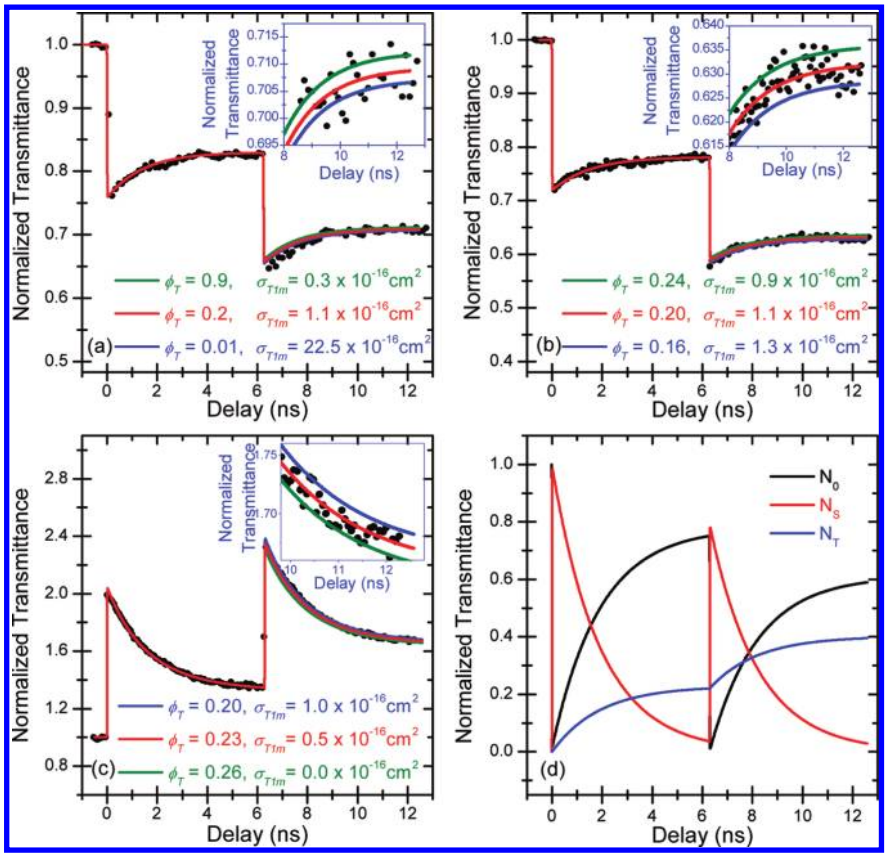

Figure 6. Experimental results and theoretical fitting for SiNc: (a) C = 2.1 mM (T_L = 0.7) and F = 11 mJ/cm^2 (E = 1 μJ, w_0 = 75 μm) in each pump; (b) C = 0.36 mM (T_L = 0.94), F = 100 mJ/cm^2 (E = 15 μJ, w_0 = 95 μm) in each pump. Pumping wavelength is 532 nm; σ_{S1n} = 32 × 10^{-18} cm^2; τ_S = 1.5 ns. (c) Experimental results and theoretical fitting for SiNc at 770 nm; C = 15 μM (T_L = 0.3), F = 0.84 mJ/cm^2 (E = 0.7 μJ, w_0 = 230 μm) in the first and F = 0.92 mJ/cm^2 (E = 0.7 μJ, w_0 = 220 μm) in the second pump; σ_{S1n} = {4.0 ± 0.2} × 10^{-16} cm^2; τ_S = 1.5 ns; and (d) population dynamics for case (c). The insets show three curves that fit the data within the experimental errors, indicating accuracy under these experimental conditions.

itself. Ophir PD10-PJ-SH-V2 detectors were used as signal and reference while, absolute energy of pump was measured with Ophir PD10-SH-V2 detector.

For femtosecond DPP experiments, a Ti:Sapphire amplified system (Clark-MXR, CPA 2011) was used at 780 nm, 1 kHz repetition rate, with a pulse width of ~150 fs (fwhm) determined by second-order autocorrelation. A schematic similar to that shown in Figure 5 was used, but the probe pulse was generated by focusing a 780 nm pulse into a 1 cm water cell to create a white-light continuum,[17] and a narrow band-pass interference filter (~10 nm) was used to select 710 nm for the probe. Pump pulses at 710 nm were generated from an OPG/A (Light Conversion, TOPAS-800). Spot sizes of both pump beams were measured by knife-edge scans to be ~120 μm (HW/e^2 M) and 20 μm (HW/e^2 M) for the probe spot size. The probe energy was fixed to ~200 pJ (F ≈ 0.032 mJ/cm^2), again small enough to prevent nonlinear effects induced by the probe. Pump beam was modulated with a mechanical chopper at 283 Hz that was synchronized with the output from the laser. Signal was recorded using silicon detector and lock-in amplifier.

Shown in Figure 5, the output of the picosecond laser system was first split by a 90:10 beam splitter, BS_1, into a pump (black lines) and probe (red lines). The pump was then split into two pumps with a 50:50 beamsplitter, BS_2, with different path lengths (mirror, M_2, can be translated), then recombined with a separation of ~6.5 ns and ~750 ps in the picosecond and femtosecond setups, respectively. The polarization of the pump beams was set using a half-waveplate/polarizer combination, HWP_1/P_1, that was also used to control the two pumps' energies before being focused by lens (L_1) onto the sample and ultimately blocked by aperture A. The probe beam was then sent through an additional half-waveplate/polarizer combination, HWP_2/P_2, to control the probe energy and, most importantly, to set the polarization of the probe at 54.7 (the "magic angle") with respect to those of the pumps to avoid pump-induced orientational effects.[37] After propagating through a 15 ns delay line, constructed from two corner cubes, CC_1 and CC_2, and a 0.5 m translation stage, the beam was then sent back to a 50:50 beamsplitter, BS_3. A reference 50:50 beamsplitter, BS_4, was used to monitor the energy on the sample, and lens, L_2, was used to focus the probe within the pumps spot size. The probe was sent through a final polarizer, P_3, set at the probe polarization to reduce scattering from the pumps, and onto a signal detector to monitor the transmitted energy using lens, L_3. Transmittance through the sample was the ratio of energy on the signal detector to the energy on the reference detector. All experiments were performed in 1 mm optical quartz cells.

4. RESULTS

The influence of fluence and concentration in the RSA region was shown by performing DPP measurements on SiNc samples at 532 nm (σ_{S01} = 2.8 × 10^{-18} cm^2; see absorption spectrum in Figure 4). Three samples were prepared with different concentrations for studies with different pump fluences and

were performed in different spectral regions. For the first sample of SiNc with the largest concentration, C = 2.1 mM, and F = 11 mJ/cm^2 in each pump, the first drop in transmittance was ~25−30%; see Figure 6a. To obtain the same change in transmittance for the second SiNc sample with smaller concentration, C = 0.36 mM, the pump fluence was increased to F = 100 mJ/cm^2 in each pump; see Figure 6b. Fitting the transmission curve for the first pump, the constant κ was determined to be $\{22.5 \pm 0.7\} \times 10^{-18}$ cm^2. As shown in the inset of Figure 6a, the fitting of experimental results for triplet state parameters for the first sample yields a very large error (more than 90%) in separating σ_{T1m} from ϕ_T, showing a major limitation of the DPP. As predicted, the second sample of SiNc, prepared with a smaller concentration and pumped with a larger fluence, allows for a unique determination of $\phi_T = \{0.21 \pm 0.04\}$ and $\sigma_{T1m} = \{1.1 \pm 0.2\} \times 10^{-16}$ cm^2 with significantly reduced errors and is in complete agreement with previously reported values.[30,31]

To allow the use of smaller pump fluences, the wavelength of operation was moved to a region of large linear absorption. It should be noted that, for photochemically unstable samples, a flow cell is recommended to exchange the solution in the focal volume with undamaged dye solution. A commonly used means of gauging photoinduced decomposition is monitoring the linear absorption spectra for a change of ≤10% (that of the photodamaged area under the spectrum divided by the initial, undamaged area under the spectrum).

The third sample of SiNc was prepared for SA studies by tuning the excitation pump wavelength to 770 nm, close to the linear absorption peak at 774 nm ($\sigma_{S01} = 12.5 \times 10^{-16}$ cm^2; Figure 4); see Figure 6c. Choosing the wavelength of operation slightly above the peak of linear absorption allows stimulated emission to be ignored from eqs 1 and 2 due to small overlap with fluorescence spectrum. Both the dye concentration and the pump fluences were much smaller for this experiment, with C = 15 μM and F = 0.84 mJ/cm^2 in the first and F = 0.92 mJ/cm^2 in the second pump. Again, constant κ was determined from the first pump to be $\{-2.7 \pm 0.6\} \times 10^{-16}$ cm^2. Fitting the experimental results for the second pump yields $\phi_T = \{0.23 \pm 0.03\}$, which is in agreement with the value obtained from the RSA measurements. The value of the TT cross section is $\sigma_{T1m} = \{0.5 \pm 0.3\} \times 10^{-16}$ cm^2. Figure 6d shows population dynamics for SiNc performed in the SA regime. We can see that in this case, even with the smallest pump fluence, the ground state is nearly completely depleted. A larger error in the determination of σ_{T1m} is due to the dominance of linear absorption is this region, $\sigma_{S01} = 12.5 \times 10^{-16}$ cm^2, over an order of magnitude larger than σ_{T1m}. However, because ϕ_T is constant for all wavelengths, σ_{T1m} can be determined from a separate pump probe measurement at other wavelengths once ϕ_T has been determined. A value of $\phi_T = \{0.23 \pm 0.03\}$, determined from DPP in the SA regime, together with a value of $\kappa = \{22.5 \pm 0.7\} \times 10^{-18}$ cm^2, determined from a single pump−probe experiment at 532 nm in the RSA regime, yields a value of σ_{T1m} for 532 nm with reasonable accuracy, $\sigma_{T1m} = \{100 \pm 10\} \times 10^{-18}$ cm^2. This shows that accurate results are obtainable with pump fluences that are $10^2\times$ less than in RSA measurements. When the investigated dyes are not photochemically stable and only exist in small research quantities, significant benefit in determining ϕ_T is gained by moving the DPP to the SA regime.

Utilizing DPP in the SA regime, ϕ_T was measured for SD 7517 (Figure 4) at two different wavelengths, 640 and 660 nm (Figure 7), with linear absorption cross sections of 5.1 and 12.1 $\times 10^{-16}$ cm^2, respectively. Again, wavelengths were chosen so

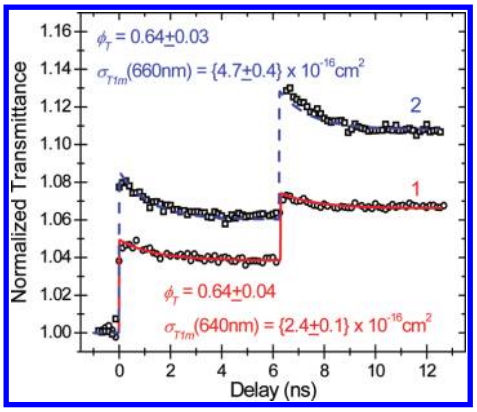

Figure 7. DPP experimental results and theoretical fitting for SD 7517: Pump wavelength at (1) 640 nm (red fit); $\sigma_{S01} = 5.1 \times 10^{-16}$ cm^2; $\sigma_{S1n} = \{2.8 \pm 0.2\} \times 10^{-16}$ cm^2; C = 6.8 μM (T_L = 0.8); F = 0.32 mJ/cm^2 (E = 0.1 μJ, w_0 = 140 μm) in the first and F = 0.52 mJ/cm^2 (E = 0.1 μJ, w_0 = 110 μm) in the second pump; and pump wavelength at (2) 660 nm (blue-dash fit); $\sigma_{S01} = 12.1 \times 10^{-16}$ cm^2; $\sigma_{S1n} = \{5.8 \pm 0.2\} \times 10^{-16}$ cm^2; C = 3 μM (T_L = 0.8); F_1 = 0.5 mJ/cm^2 (E = 0.5 μJ, w_0 = 250 μm) in the first and F_2 = 0.55 mJ/cm^2 (E = 0.5 μJ, w_0 = 240 μm) in the second pump. In both cases, τ_S = 1.4 ns.

that there is no influence of stimulated emission. As shown in Figure 7, both experiments give indistinguishable values for $\phi_T = \{0.64 \pm 0.03\}$, while $\sigma_{T1m} = \{2.4 \pm 0.2\} \times 10^{-16}$ cm^2 at 640 nm and $\sigma_{T1m} = \{4.7 \pm 0.4\} \times 10^{-16}$ cm^2 at 660 nm. At both wavelengths, the values obtained for σ_{T1m} are again smaller than the ground-state absorption cross section, as expected. These results show that performing the DPP in the SA regime often yields the most accurate determination of ϕ_T. Single pump−probe measurements can now be utilized to determine the wavelength dependence of σ_{T1m} (after an accurate determination of ϕ_T has been made).

We now consider a metal−organic system with an ultrafast ISC. Ruthenium phthalocyanines and naphthalocyanines are known to exhibit very fast ISC rates, with ISC time scales on the order of a few picoseconds,[34,35] so DPP characterization of RuNc-G3 requires the use of femtosecond pulses. Typically, femtosecond sources are avoided for triplet yield studies due to their increased irradiance as compared to picosecond pulses at the same fluence and their typically faster pulse repetition rates, which both may lead to faster photodecomposition. However, a DPP measurement in the SA regime allows significantly lower pump fluence, reducing the probability of dye photoinduced decomposition. Experiments were performed at a pump wavelength of 710 nm, which is close to the 715 nm absorption peak of this molecule shown in Figure 4. Theoretical fitting was performed using the full set of propagation and rate equations for the five-level system, Figure 1 and eqs 1 and 2. Fitted results are shown in Figure 8a, and their corresponding population dynamics are shown in Figure 8b. The values obtained are: $\phi_T = \{0.97 \pm 0.01\}$, $\sigma_{S1n} = \{3.5 \pm 0.1\} \times 10^{-16}$ cm^2, $\sigma_{T1m} = \{3.4 \pm 0.1\} \times 10^{-16}$ cm^2, and τ_S = 5.3 ps. Scanning with greater temporal resolution around the zero delay of the first pump (shown in the inset of Figure 8a) allows a determination of the singlet parameters using femtosecond pulses.

Figure 8a demonstrates interesting dynamics. There is a small change in transmittance after the first and second

dx.doi.org/10.1021/jp301051u | J. Phys. Chem. A 2012, 116, 4833−4841

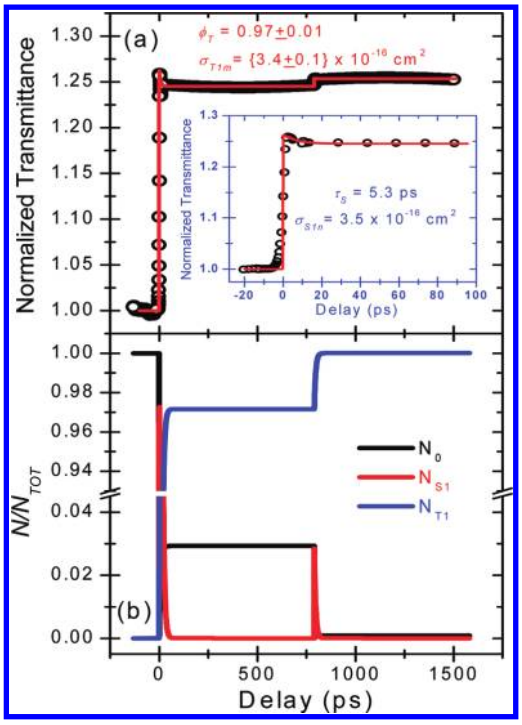

Figure 8. (a) DPP and fitting results for RuNc-G3 at a pump of 710 nm ($\sigma_{S01} = 6.6 \times 10^{-16}$ cm^2), $C = 12$ μM ($T_L = 0.6$), $F = 3.4$ mJ/cm^2 ($E = 0.7$ μJ, $w_0 = 115$ μm) in each pump, and $\tau_S = 5.3$ ps. Inset: Greater temporal resolution scan showing S_1 dynamics for the first pump pulse only. (b) DPP population dynamics for the ground, first excited singlet, and triplet states for RuNc-G3 for the conditions in (a).

pumping pulses. The calculated population dynamics for the ground, first excited singlet, and triplet states are shown in Figure 8b. It is seen that the fluence of the first pump is large enough to almost completely deplete the ground state. Because ϕ_T is almost unity, all excited population moves to the triplet state, T_1, immediately after the first pump, and therefore the influence of the second pump is very small.

Now we can compare these results to what is obtained from the singlet depletion method ignoring TT absorption for the previous three examples of DPP in the SA region. The values determined (singlet depletion method) for ϕ_T are: 0.22 for SiNc, 0.39 for SD 7517, and 0.45 for RuNc-G3. As we can see, the error is smallest for SiNc because σ_{T1m} is an order of magnitude smaller than σ_{S01}. For SD 7517 and RuNc-G3 the error is 50−60%, which means that TT absorption cannot be ignored for these two compounds and the singlet depletion method is not accurate.

5. CONCLUSIONS

Limitations in the accuracy of the double pump−probe (DPP) technique for independently determining the triplet quantum yield, ϕ_T, and triplet cross section, σ_{T1m}, have been identified, and we have described methods of optimizing the technique in light of these limitations. This optimization is particularly important for dyes that undergo photoinduced decomposition by allowing lower fluences to be used. The limitations are connected primarily with attempts to perform DPP in regions of small linear absorption where materials may exhibit RSA. In the RSA regime, the fraction of ground-state population moved to the triplet state is small at relatively small pump fluences, especially for large dye concentrations, thus leading to low sensitivity and poor accuracy of the DPP. Under these conditions, the values of ϕ_T and σ_{T1n} cannot be accurately decoupled. To successfully decouple ϕ_T and σ_{T1m}, a significant fraction of initial ground-state population has to be redistributed to the triplet state. In the RSA regime, where ground-state absorption is small, this can be achieved only by increasing the pump fluence and lowering the dye concentration. This approach is not always practical due to photochemical instability of many organic molecules. Analytical simulations, confirmed by experimental results, show that when the pumping wavelength is moved to the SA regime, even a small excitation fluence can significantly depopulate the ground state. A larger fraction of the ground-state population moved to the triplet state results in greatly improved accuracy in the determination of ϕ_T. Although ϕ_T can be determined accurately in this region, measurements of σ_{T1m} are still inaccurate because κ involves the product of the difference. Precise determination of σ_{T1m} in the RSA region, useful for many applications, requires a separate measurement at the desired wavelength with knowledge of ϕ_T.

Using this optimized DPP method, we have characterized the triplet dynamics of two new dyes, SD 7517 and RuNc-G3, in a spectral region close to the linear absorption peak. The experimental error in determining ϕ_T is a few percent in both cases, showing the usefulness of the DPP.

■ ASSOCIATED CONTENT

Supporting Information

Details of single pump−probe experiment, dependence of double pump−probe accuracy on different experimental parameters, and additional figures. This material is available free of charge via the Internet at http://pubs.acs.org.

■ AUTHOR INFORMATION

Corresponding Author

*E-mail: ewvs@creol.ucf.edu.

Notes

The authors declare no competing financial interest.

■ ACKNOWLEDGMENTS

We gratefully acknowledge support of the U.S. Army Research Laboratory and the U.S. Army Research Office (50372-CH-MUR), the Air Force Office of Scientific Research (FA9550-10-1-0558), the Office of Naval Research (MORPH N00014-06-1-0897), the Science and Technology Center Program of the National Science Foundation (DMR-0120967), and the Israel Ministry of Defense (993/54250-01). We thank Matthew Reichert and Lazaro A. Padilha for useful input.

■ REFERENCES

(1) Hollins, R. C. Materials for optical limiters. *Curr. Opin. Solid State Mater. Sci.* **1999**, *4*, 189−196.

(2) Hughes, S.; Spruce, G.; Wherrett, B. S.; Kobayashi, T. Comparison between the optical limiting behavior of chloroaluminum phthalocyanine and a cyanine dye. *J. Appl. Phys.* **1997**, *81*, 5905−5912.

(3) Sanghadasa, M.; Shin, I.-S.; Clark, R. D.; Guo, H.; Penn, B. G. Optical limiting behavior of octa-decyloxy metallo-phthalocyanines. *J. Appl. Phys.* **2001**, *90*, 31−37.

(4) Kappaun, S.; Slugovc, C.; List, E. J. W. Phosphorescent organic light-emitting devices: Working principle and iridium based emitter materials. *Int. J. Mol. Sci.* **2008**, *9*, 1527−1547.

(5) Tsuzuki, T.; Tokito, S. Phosphorescent organic light-emitting devices using Pt complexes as emitting materials. *Proc. Int. Symp. Super-Functionality Organic Devices, IPAP Conf. Series 6*, 99−103.
(6) Augustin, C. M.; Oswald, B.; Wolfbeis, O. S. Time-resolved luminescence energy transfer immunobinding study using a ruthenium−ligand complex as a donor label. *Anal. Biochem.* **2002**, *305*, 166−172.
(7) Ermilov, E. A.; Tannert, S.; Werncke, T.; Choi, M. T. M.; Ng, D. K. P.; Roder, B. Photoinduced electron and energy transfer in a new porphyrin−phthalocyanine triad. *Chem. Phys.* **2006**, *328*, 428−437.
(8) Macdonald, I. J.; Dougherty, T. J. Basic principles of photodynamic therapy. *J. Porphyrins Phthalocyanines* **2001**, *5*, 105−129.
(9) Bonnett, R. Photosensitizers of the porfyrin and phthalocyanine series for photodynamic therapy. *Chem. Soc. Rev.* **1995**, *24*, 19−33.
(10) Redmond, R. W.; Gamlin, J. N. A compilation of singlet oxygen yields from biologically relevant molecules. *Photochem. Photobiol.* **1999**, *70*, 391−475.
(11) Schweitzer, C.; Schmidt, R. Physical mechanisms of generation and deactivation of singlet oxygen. *Chem. Rev.* **2003**, *103*, 1685−1757.
(12) Seixas de Melo, J.; Silva, L. M.; Arnaut, L. G.; Becker, R. S. Singlet and triplet energies of α-oligothiophenes: A spectroscopic, theoretical, and photoacoustic study: Extrapolation to polythiophene . *J. Chem. Phys.* **1999**, *111*, 5427−5434.
(13) Detty, M. R.; Merkel, P. B. Chalcogenapyrylium dyes as potential photochemotherapeutic agents. Solution studies of heavy atom effects on triplet yields, quantum efficiencies of singlet oxygen generation, rates of reaction with singlet oxygen, and emission quantum yields. *J. Am. Chem. Soc.* **1990**, *112*, 3845−3855.
(14) Lament, B.; Karpiuk, J.; Waluk. Determination of triplet formation efficiency from kinetic profiles of the ground state recovery. *J. Photochem. Photobiol. Sci.* **2003**, *2*, 267−272.
(15) King, S. M.; Rothe, C.; Dai, D.; Monkman, A. P. Femtosecond ground state recovery: measuring the intersystem crossing yield of polyspirobifluorene. *J. Chem. Phys.* **2006**, *124*, 234903−234906.
(16) Seixas de Melo, J.; Silva, L. M.; Arnaut, L. G.; Becker, R. S. Singlet and triplet energies of α-oligothiophenes: A spectroscopic, theoretical, and photoacoustic study: Extrapolation to polythiophene. *J. Chem. Phys.* **1999**, *111*, 5427−5434.
(17) Negres, R. A.; Przhonska, O. V.; Hagan, D. J.; Van Stryland, E. W.; Bondar, M. V.; Slominsky, Y. L.; Kachkovski, A. D. The nature of excited-state absorption in polymethine and squarylium molecules. *IEEE J. Sel. Top. Quantum Electron* **2001**, *7*, 849−863.
(18) Swatton, S. N. R.; Welford, K. R.; Hollins, R. C. A time resolved double pump−probe experimental technique to characterize excited-state parameters of organic dyes. *Appl. Phys. Lett.* **1997**, *71*, 10−12.
(19) McEwan, K. J.; Bourhill, G.; Robertson, J. M.; Anderson, H. L. The nonlinear optical characterization of meso-substituted porphyrin dyes. *J. Nonlinear Opt. Phys.* **2000**, *9*, 451−486.
(20) Krivokapic, A.; Anderson, H. L.; Bourhill, G.; Ives, R.; Clark, S.; McEwan, K. J. Meso-tetra-alkynyl porphyrins for optical limiting - Survey of Group III and IV metal complexes. *Adv. Mater.* **2001**, *13*, 652−656.
(21) Schell, J.; Ohlmann, D.; Brinkmann, D.; Lévy, R.; Joucla, M.; Rehspringer, J. L.; Hnerlage, B. Reverse saturable absorption in C60-doped porous glasses studied by single- and double-pulse pump−probe experiments . *J. Chem. Phys.* **1999**, *111*, 5929−5937.
(22) Webster, S.; Peceli, D.; Hu, H.; Padilha, L. A.; Przhonska, O. V.; Masunov, A. E.; Gerasov, A. O.; Kachkovski, A. D.; Slominsky, Y. L.; Tolmachev, A. I.; Kurdyukov, V. V.; Viniychuk, O. O.; Barrasso, E.; Lepkowicz, R.; Hagan, D. J.; Van Stryland, E. W. Near-unity quantum yields for intersystem crossing and singlet oxygen generation in polymethine-like molecules: Design and experimental realization. *J. Phys. Chem. Lett.* **2010**, *1*, 2354−2360.
(23) Patterson, F. G.; Lee, H. W. H.; Wilson, W. L.; Fayer, M. D. Intersystem crossing from singlet states of molecular dimers and monomers in mixed molecular crystals: picosecond stimulated photon echo experiments. *Chem. Phys.* **1984**, *84*, 51−60.
(24) Gilmore, E. H.; Gibson, G. E.; McClure, D. S. Absolute quantum efficiencies of luminescence of organic molecules in solid solution. *J. Chem. Phys.* **1952**, *20*, 829−836.
(25) Perry, J. W. Organic and metal-containing reverse saturable absorbers for optical limiters. In *Nonlinear Optics of Organic Molecules and Polymers*; Nalwa, H. S., Miyata, S., Eds.; CRC Press: New York, 1997; pp 813−840.
(26) Van Veenendaal, M.; Chang, J.; Fedro, A. Model of ultrafast intersystem crossing in photoexcited transition-metal organic compounds. *J. Phys. Rev. Lett.* **2010**, *104*, 067401.
(27) Hedley, G. J.; Ruseckas, A.; Samuel, I. D. W. Ultrafast intersystem crossing in a red phosphorescent iridium complex. *J. Phys. Chem. A* **2009**, *113*, 2−4.
(28) Ramakrishna, G.; Goodson, T.; Rodgers-Haley, J. E.; Cooper, T. M.; McLean, D. G.; Urbas, A. Ultrafast intersystem crossing: Excited state dynamics of platinum acetylide complexes. *J. Phys. Chem. C* **2009**, *113*, 1060−1066.
(29) Peceli, D.; Webster, S.; Fishman, D.; Cirloganu, C.; Pattanaik, H.; Hu, H.; Przhonska, O. V.; Kurdyukov, V. V.; Slominsky, Y. L.; Tolmachev, A. I.; Kachkovski, A. D.; Dasari, R. R.; Barlow, S.; Marder, S. R.; Hagan, D. J.; Van Stryland, E. W. Advance in double pump-probe technique for triplet quantum yield determination in CLEO:2011 - Laser Applications to Photonic Applications, OSA Technical Digest (CD); Optical Society of America, 2011, paper CTuY4.
(30) Dogariu, A. Spectral and temporal response of optical nonlinearities. Ph.D. Thesis, University of Central Florida, Source DAI-B 58/02, 1997; 256 pages.
(31) Firey, P. A.; Sounik, J. R.; Ford, W. E.; Kenney, M. E.; Rodgers, M. A. J. Silicon naphthalocyanine triplet state and oxygen. A reversible energy-transfer reaction. *J. Am. Chem. Soc.* **1988**, *110*, 7626−7630.
(32) Xia, T.; Hagan, D. J.; Dogariu, A.; Said, A. A.; Van Stryland, E. W. Optimization of optical limiting devices based on excited-state absorption. *Appl. Opt.* **1997**, *36*, 4110−4122.
(33) Kobyakov, A.; Hagan, D. J.; Van Stryland, E. W. Analitical approach to dynamics of reverse saturable absorbers. *J. Opt. Soc. Am. B* **2000**, *17*, 1884−1893.
(34) Dasari, R. R.; Sartin, M. M.; Cozzuol, M.; Barlow, S.; Perry, J. W.; Marder, S. R. Synthesis and linear and nonlinear absorption properties of dendronised ruthenium(II) phthalocyanine and naphthalocyanine. *Chem. Commun.* **2011**, *47*, 4547−4549.
(35) Guez, D.; Markovitsi, D.; Sommerauer, M.; Hanack, M. Photophysical properties of a ruthenium(II) phthalocyanine. *Chem. Phys. Lett.* **1996**, *249*, 309−313.
(36) Solovyov, K. N.; Borisevich, E. A. Intramolecular heavy-atom effect in the photophysics of organic molecules. *Phys.-Usp.* **2005**, *48*, 231−253.
(37) Lessing, H. E.; Von Jena, A. Separation of rotational diffusion and level kinetics in transient absorption spectroscopy. *Chem. Phys. Lett.* **1976**, *42*, 213−217.